Simple Simulations of DNA Condensation

Mark J. Stevens
Sandia National Laboratory, P.O. Box 5800, MS 1111, Albuquerque, New Mexico 87185 USA

ABSTRACT Molecular dynamics simulations of a simple, bead-spring model of semiflexible polyelectrolytes such as DNA are performed. All charges are explicitly treated. Starting from extended, noncondensed conformations, condensed structures form in the simulations with tetravalent or trivalent counterions. No condensates form or are stable for divalent counterions. The mechanism by which condensates form is described. Briefly, condensation occurs because electrostatic interactions dominate entropy, and the favored coulombic structure is a charge-ordered state. Condensation is a generic phenomenon and occurs for a variety of polyelectrolyte parameters. Toroids and rods are the condensate structures. Toroids form preferentially when the molecular stiffness is sufficiently strong.

INTRODUCTION

The high degree of packing necessary to package DNA into cells is well known (Bloomfield, 1996). Typically, DNA is orders of magnitude longer than any dimension of the cell in which it resides. Since DNA is a highly charged polyelectrolyte, packing DNA into a small volume requires overcoming an enormous Coulomb barrier. It is only partially understood how this can occur. This article treats the general case of condensing highly charged, semiflexible polyelectrolytes by multivalent ions. The prime example is fitting of DNA into a bacteriophage's capsid, since bacteriophages are simple systems that do not possess condensing proteins (histones) present in eukaryotic cells.

The purpose of this work is to demonstrate that electrostatic interactions provide a general mechanism to condense semiflexible polyelectrolytes such as DNA. It is well known experimentally that multivalent ions can condense DNA into toroids and rods (Bloomfield, 1996, 1991; Kleinschmidt et al., 1962; Fang and Hoh, 1998). Although these experiments have yielded many important clues to the important interactions in DNA condensation, understanding of these interactions remains incomplete. The key issue is how the net electrostatic interaction between like charged monomers changes from repulsive to attractive. For, as long as the net interaction is repulsive, the polyelectrolyte cannot condense.

Condensation is directly demonstrated for semiflexible polyelectrolytes such as DNA with multivalent counterions, using molecular dynamics simulations of simple, model polyelectrolytes. Once condensation is demonstrated, the nature of the condensates and the condensation process are investigated. How multivalent ions can overcome the large Coulomb repulsion between the charged monomers is explained. The subtle competition between electrostatic interactions and entropy is noted in the failure of divalent counterions yielding condensates. The effect of molecular stiffness on the condensate structure is also treated.

Received for publication 8 June 2000 and in final form 21 September 2000.

Address reprint requests to Dr. Mark J. Stevens, Sandia National Laboratory, MS 1111, P.O. Box 5800, MS 1111, Albuquerque, New Mexico 87185. Tel.: 505-844-1937; Fax: 505-845-7442; E-mail: msteve@sandia.gov.

0006-3495/01/01/130/10 $2.00

Background

A net attraction between like-charged macroions is somewhat counterintuitive, but it is known to occur in certain circumstances (Lyubartsev and Nordenskiöld, 1995; Kjellander and Marčelja, 1984; Stevens and Robbins, 1990). Calculations of electrostatic interactions involving multivalent ions are difficult. The traditional approximations, such as Debye-Hückel and Poisson-Boltzmann (PB), break down in these circumstances (Kjellander and Marčelja, 1984; Stevens and Robbins, 1990). These approximations are valid primarily for Coulomb interactions weak in comparison with k_BT, where k_B is the Boltzmann constant and T is the temperature. This is not true for DNA and becomes even less true in the presence of multivalent ions. Both of these theories can only yield repulsive interactions between chain segments (Neu, 1999; Sader and Chan, 1999). Thus, no condensation can occur.

Treatment of the complex interactions for highly charged macroions of simple geometry (e.g., plates, cylinders) has been developed (Kjellander and Marčelja, 1984; Stevens and Robbins 1990; Ha and Liu, 1997). A short-range attraction between two macroions is possible and understood. DNA is often treated as a charged cylinder. Simulations have found attraction between charged cylinders (Grønbech-Jensen et al., 1997; Lyubartsev and Nordenskiöld, 1995) and stiff polyelectrolytes (Stevens, 1999) in the presence of multivalent ions. This attraction has been ascribed to correlated fluctuations of the counterions (Ha and Liu, 1997; Ray and Manning, 1994). Ha and Liu (1997) developed an internally consistent field theory for systems of parallel, charged cylinders. Their theory shows that condensed counterions induce charge fluctuations along the rods, giving rise to attractive interactions. Self-attraction in flexible polyelectrolytes has also been shown to occur (Stevens and Kremer, 1995; Schiessel and Pincus, 1998; Brilliantov et al., 1998). Brilliantov et al. (1998) showed

that flexible polyelectrolytes can collapse for strong Coulomb interactions, using an extension to polymers of density functional theory methods (Stevens and Robbins, 1990). This is in agreement with earlier simulations (Stevens and Kremer, 1995).

A important phenomenon for highly charged polyelectrolytes such as DNA is counterion condensation (Manning, 1969; Oosawa, 1971). For a sufficiently charged polyelectrolyte, some of the counterions become effectively bound. Manning's solution of the Debye-Hückel equation shows that when the ratio of the Bjerrum length, λ to the charge separation distance, a is greater than one, then enough counterions condense onto the polyelectrolyte in order to reduce the effective ratio $\xi = \lambda/a$ to be equal to 1. Counterion condensation occurs for all highly charged polyelectrolytes, including DNA, independent of the counterion valence. Thus, condensation of the polyelectrolyte requires more than counterion condensation.

THEORY

A simple description of the physical source for the attractive interactions can be given in terms of the one-component plasma (OCP), which consists of a single charged species in a uniform neutralizing background (Baus and Hansen, 1980). The OCP can be described in terms of a single parameter,

$$\Gamma = \lambda/a_p, \tag{1}$$

where a_p is the average interparticle separation, defined in terms of the density, ρ, as $ap = 3/(4\pi\rho)^{1/3}$. The OCP parameter Γ is similar to the quantity ξ; the difference is that OCP refers to a three-dimensional system and ξ to a one-dimensional system. Physically, the parameters Γ and ξ define the relative strength of the typical Coulomb pair interaction to the entropic interaction. When either quantity is greater than one such as when counterion condensation occurs, the Coulomb interactions dominate the entropic interactions. Small Γ is equivalent to low density. Fig. 1 gives the normalized pressure, $P^* = \lambda^3/k_BT$ vs. Γ The OCP pressure becomes the ideal gas law at small Γ,

$$P^* \simeq \Gamma^3 \sim \rho. \tag{2}$$

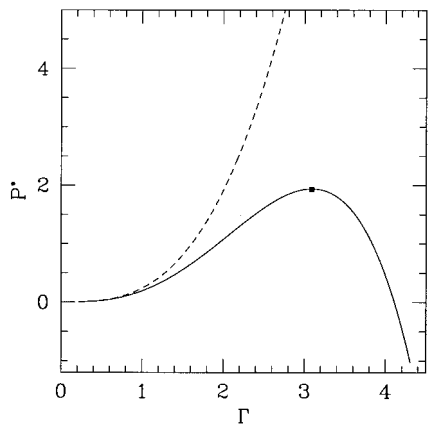

FIGURE 1 The pressure for the one-component plasma (OCP) as a function of the parameter $\Gamma = \lambda/a_p$, where λ is the Bjerrum length and a_p is the average interparticle spacing. The dotted line gives the pressure calculated in the PB approximation. The pressure is calculated from the free energy given in Brami et al. (1979), which was fitted to a combination of Monte Carlo data and hypernetted chain calculations.

In this regime the PB approximation is valid, because entropy is the dominant interaction. As Fig. 1 shows, at $\Gamma \sim 1$, the PB approximation breaks down; the pressure calculated in the PB approximation significantly deviates from the correct value. Furthermore, the PB pressure is always positive (Neu, 1999; Sader and Chan, 1999).

As Γ increases, the Coulomb interactions become more dominant, until at $\Gamma = 3.09$ a mechanical instability occurs. Because the equilibrium Coulomb energy is negative and decreasing the volume brings the particles closer together, the Coulomb energy decreases with decreasing volume. Minimizing just the Coulomb interactions would collapse the system. At lower Γ, sufficiently strong entropic interactions stabilize the system. However, at $\Gamma = 3.09$, entropy cannot stop the volume decreasing, and the system will shrink until steric repulsions stop the contraction. In polyelectrolytes, this instability is related to counterion condensation (Stevens and Robbins, 1990). If $\Gamma = 4.1$ can be reached without steric repulsion occurring, then the pressure is negative and the system has a global (self) attraction. For much higher Γ, the system undergoes a phase transition much like an ionic crystal such as NaCl. A single polyelectrolyte can collapse due to this global attraction, if the equivalent Γ achieves these large values. In this picture, DNA condensation is a result of the Coulomb interactions being sufficient strong (large Γ) that they dominate entropic interactions and can achieve a charged-ordered state that has the lowest Coulomb energy. In macroion systems, the signature for this transition is that the equilibrium charge distribution becomes highly correlated with alternating negative and positive charges.

DNA condensation typically occurs for counterion valences of 3 or larger. The importance of multivalency is that it increases the magnitude of the Coulomb interactions. In the OCP picture (Stevens and Robbins, 1990; Stevens et al., 1996) the Bjerrum length is written

$$\lambda = z_c^2 e^2/\epsilon k_B T, \tag{3}$$

where z_c is the counterion valence and ε is the dielectric constant of water. Thus, trivalent counterions increase the Bjerrum length by a factor of 9. This enables the net attraction to occur before the steric repulsion enters. For monovalent and divalent ions, the Coulomb interactions are not strong enough to counter entropic effects. Thus, condensates do not form for low valence counterions.

A simple calculation of Γ for polyelectrolyte collapse produces a rather reasonable number despite some strong simplifications (cf. Brilliantov et al., 1998). In this calculation, Γ is calculated based on the condensed counterion volume. The density of condensed counterions involves just the volume near the polyelectrolyte. The volume can be estimated to be a cylinder about the polyelectrolyte with a diameter containing counterions within a single counterion diameter of the polyelectrolyte. For $z_c \geq 3$, the simulations show this is a good estimate of the volume. Writing the polyelectrolyte radius as R and the counterion diameter as d, then the volume is $V = \pi(R + d)^2L$. The polyelectrolyte length is $L = (N - 1)a$, where N is the number of charged monomers and a is the charge monomer separation distance. Taking all counterions as condensed, then the counterion density is

$$\rho = \frac{N/z_c}{4\pi(R + d)^2(N - 1)a} \simeq (4\pi(R + d)^2 a z_c)^{-1}. \tag{4}$$

Then,

$$\Gamma = \lambda/(3(R + d)^2 a z_c)^{1/3}. \tag{5}$$

Using $\lambda = 7.1$ Å, $R = 10$ Å, $d = 4$ Å, and $a = 1.7$ Å, one obtains $\Gamma = 7.1$ for $z_c = 4$ and $\Gamma = 2.0$ for $z_c = 2$. For $z_c = 2$, the condensed counterion volume may in fact be larger, but this just reduces Γ further. Thus,

tetravalent counterions are in the attractive regime, but divalent ions are just in the counterion condensation regime.

Using molecular dynamics simulations, no approximations are necessary as in analytic calculations. The interactions necessary for condensation can be conclusively determined. In addition, other useful information about these interactions is obtained. Because the persistence length of DNA is large, the polymer lengths that can be studied are smaller than in DNA. The simulations will treat several model polyelectrolytes that otherwise have physical parameters in a regime similar to DNA. Three key lengths are the charge separation distance a, the intrinsic persistence length L_p, and the chain length L. The important relation that holds for DNA is $a < Lp < L$. The model polyelectrolytes satisfy this relation. Condensation will occur independent of L so long as this relation holds. The condensate structure, however, can depend on L_p, as will be seen.

Simulation methods

A large body of work has been performed on bead-spring model polyelectrolytes (Stevens and Kremer, 1995; Stevens, 1999). Bead-spring models are necessary to treat the slow dynamics of polymers. Atomistic simulations, particularly for polyethylene, let alone DNA, cannot treat the necessary time scales. Coarse-grained simulations have already demonstrated the aggregation of multiple stiff polyelectrolytes such as single persistence length DNA or actin (Stevens, 1999).

Molecular dynamics simulations are performed on a system composed of M bead-spring chains with N beads. In the bead-spring model, the beads represent some number of monomers. In the present case of charged polymers, each bead has a single charge and thus corresponds to the set of monomers containing a single charge. The bead is given a size by the Lennard-Jones (LJ) potential.

$$U_{LJ}(r) = \begin{cases} 4\epsilon\left[\left(\frac{\sigma}{r}\right)^{12} - \left(\frac{\sigma}{r}\right)^{6} + \frac{1}{4}\right]; & r \le r_c \\ 0; & r > r_c \end{cases} \quad (6)$$

The LJ potential is cut off at $r_c = 2^{1/6}\sigma$, which yields a purely repulsive potential. All the units will be in terms of the LJ quantities, ϵ and σ.

The bond potential is the sum of two parts. The repulsive part is the LJ potential described above. The attractive part is the standard finite extensible, nonlinear elastic (FENE) potential

$$U_{FENE}(r) = -1/2kR_0^2 \ln(1 - r^2/R_0^2), \quad (7)$$

with spring constant $k = 7\ \epsilon/\text{rad}^2$, and maximum extent, $R_0 = 2\ \sigma$. The key aspect of the FENE bond potential is that it does not allow chains to cross. For the parameters used, the average bond length is $a = 1.1\ \sigma$.

The polymers are given an intrinsic stiffness by including a bond angle potential,

$$U_{angle} = k_1(\theta - \theta_0)^2 + k_2(\theta - \theta_0)^4, \quad (8)$$

where θ is the bond angle between three consecutive beads and the equilibrium value is $\theta_0 = 180°$. A few values of the spring constants k_1 and k_2 have been used. Some values of k_1 and k_2 can be found in Table 2, which lists bond angle parameter sets. When $k_2 = 0$, the intrinsic persistence length is directly proportional to k_1. Defining the persistence length as the length of n chain segments which forms an arc of 1 radian with a bond bending energy of k_BT. Then, one can derive that the intrinsic persistence length is

$$L_p = \frac{k_1 a}{k_B T} \quad (9)$$

For $k_1 = 20\ \epsilon/\text{rad}^2$, $L_p = 19\ \sigma$.

In these simulations, the counterions are explicitly treated. All charged particles interact via the Coulomb potential

$$u_{ij}(r) = q_i q_j k_B T \lambda / r, \quad (10)$$

where q_i is the charge on particle i and the Bjerrum length in water is $\lambda = 7.1$ Å. Water is treated as a uniform dielectric background. For this work, no added salt is included. For these simulations we used the particle-particle particle-mesh algorithm to calculate the long range Coulomb interactions (Hockney and Eastwood, 1988; Pollock and Glosli, 1996). Some single-chain simulations used the direct sum over all pairs.

The total energy is

$$U_{tot} = U_{LJ} + U_{bond} + U_{angle} + U_{Coulomb}. \quad (11)$$

Two polyelectrolyte parameter sets have been studied. Following much work on flexible polyelectrolytes (Stevens and Kremer, 1995), $\lambda = 3.2\ \sigma$ has been used. This yields $a = 2.5$ Å, which corresponds to synthetic polyelectrolytes such as sodium poly (styrene sulfonate). The parameters are listed in Table 1. Parameter set 2 matches DNA values. The value of $\lambda = 4.68\ \sigma$ corresponds to $a = 1.7$ Å. The monomer diameter d is set to 4 Å as this corresponds to a typical ionic diameter including hydration shells. Though DNA has a radius of about 10 Å, the key quantity is the distance of nearest approach of the monomer charge (phosphates) and the solvent ions; this distance is typically about equal to the counterion diameter.

The dynamics of the system is performed at constant temperature, $T = 1.2$, using the Langevin thermostat (Schneider and Stoll, 1985) with damping constant equal to $1/\tau$, and time step $0.015\ \tau$, where τ is the LJ time unit. The mapping of τ to seconds has yet to be done for polyelectrolytes. For neutral polystyrene, $\tau = 3.1 \times 10^{-8}$ s (Kremer and Grest, 1990). Typically, stiffer polymers have larger τ. DNA is much stiffer than polystyrene and probably has τ more than one order of magnitude larger.

In order to avoid interactions between chains, the simulations were performed at very low chain densities, typically less than or equal to $2 \times 10^{-5}\ \sigma^{-3}$. In this work, only conformations of individual molecules are the focus. Figures will show individual conformations oriented with respect to the radius of gyration tensor. Each molecule is oriented with major axis to the right and the minor axis perpendicular to the page.

For most simulations the initial conformation for each molecules in the simulation cell is created by a random walk with a stretch condition that the next nearest neighbor distance is greater than an input value, typically $2d$. The larger the value the more extended the chain is. Highly charged polyelectrolytes are typically significantly extended. The counterions are placed randomly within a volume about each molecule.

RESULTS

Condensation

The first issue to be settled is whether toroidal structures will form in these simulations. Fig. 2 shows the conformations for parameter set 1 with bond angle set 1, $N = 64$, $z_c = 4$, $k_1 = 10\ \epsilon/\text{rad}^2$, and $\rho = 1 \times 10^{-4}\ \sigma^{-3}$. Not only toroids, but also rod structures form. The rods are more common in this simulation as well as others to be discussed. The two

TABLE 1 Polyelectrolyte parameters

Set	σ	ξ	d
1	2.2	2.9	2.5
2	1.5	4.2	4.0

The lengths are given in Å.

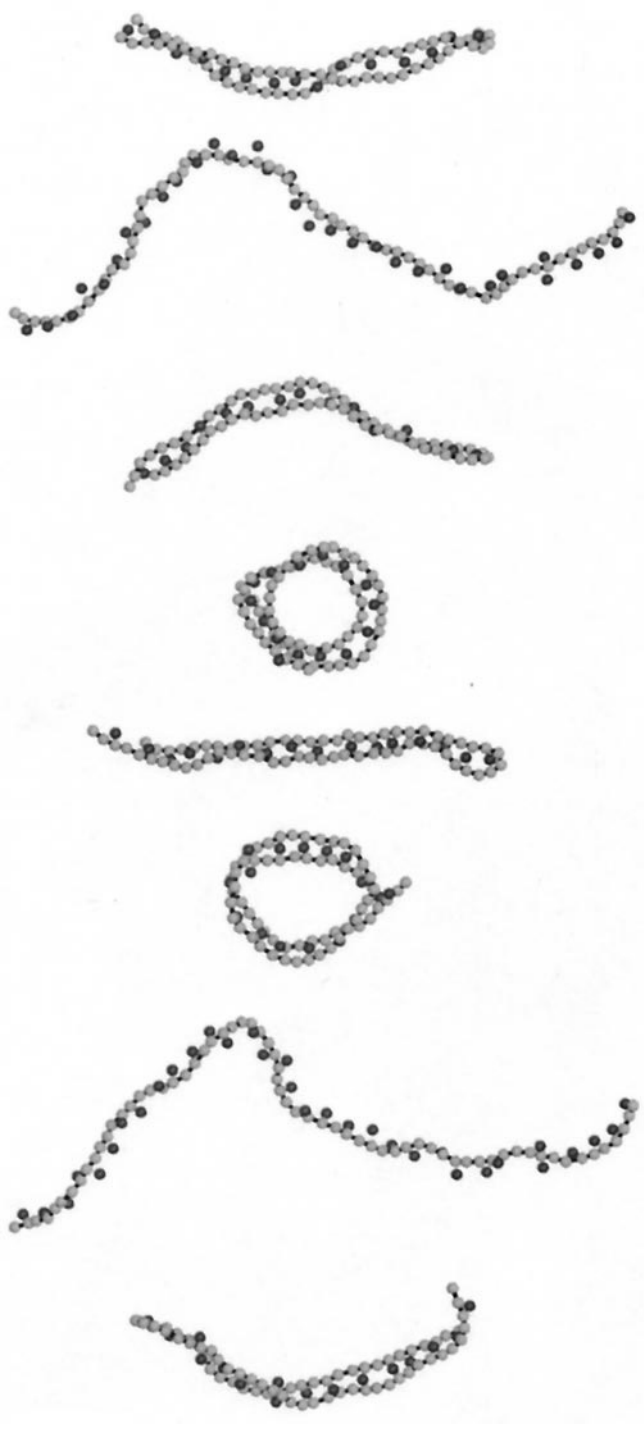

FIGURE 2 Images of structures for $N = 64$ molecules (*light spheres*) with $z_c = 4$ counterions (*dark spheres*). Both toroids and rods appear.

molecules that do not self-condense have actually aggregated; their conformations are strikingly similar because of they form a bundle pair. (In all other systems, the density was lowered to avoid pair formation.) The images are shown at time $t = 6000\ \tau$. The bottom toroid is fully formed by $t = 1200\ \tau$. The top toroid takes $5200\ \tau$ to form. All but one of the rods form before the first toroid forms.

The figure shows the (condensed) counterions, which are within $2d$ of any monomer. In general, for $z_c = 4$, all the counterions condense. While the counterions are condensed, they still move about in the volume near the polymer. In other words, the counterions are bound to the polyelectrolyte, not to some monomer. As such, they do not lose all their entropy in becoming condensed. This is very important, as divalent counterions typically fail to yield DNA condensation experimentally (Bloomfield, 1996). Divalent ions have relatively weaker Coulomb interactions than tetravalent ions and have more entropy costs since there are twice as many. Entropy wins in the divalent ion case.

Simulations performed with divalent ions do not form any condensed structures. This is not completely convincing, in that there is always the issue of whether condensation would occur if the simulation were run longer. To treat this issue, simulations have been performed starting with initial conformations near the toroid structure. The initial polyelectrolyte conformation is a spiral. The counterions are placed on a separate spiral such that they are between successive arcs of the polymer's spiral. The energy of the single conformation with counterions was calculated for varying spiral radius and pitch. The minimum energy conformation was found and used as the initial state. For parameter set 2 with bond angle set 3 and $N = 256$, one turn of the spiral has 40 beads and the pitch is $2 \times 2^{1/6}d$. This value of the pitch yields puts the counterions and charged monomers as close as possible without overlap of the LJ spheres. The spiral structure should be able to evolve easily into a toroidal structure, which is just multiple spirals that are connected and successively surround each other.

Fig. 3 shows the conformations of the 8 polyelectrolytes with divalent counterions after about 5×10^6 time steps ($7.4 \times 10^4\ \tau$) starting from the spiral conformation. Clearly the toroidal structure is not stable for the divalent system. On average, 116 out of 128 counterions per chain condense to within $2d$ of the polyelectrolytes. The polyelectrolyte with these counterions has a net negative charge. The simulations show that this net charge results in a net repulsion within the molecule and an extended structure. In comparison with the $z_c = 4$ system, more counterions are delocalized and are not screening the monomeric charges.

Whereas single polyelectrolytes with divalent counterions do not self-condense, multiple polyelectrolytes with divalent counterions will form bundles (Stevens, 1999). Counterions condensed to a bundle move throughout the bundle volume. Consequently, their entropy is much larger than the entropy of counterions condensed to a single self-condensed polyelectrolyte. For this reason, divalent ions can yield multiple polyelectrolyte condensation, but typically do not yield single molecule condensation.

For the same parameter set but with tetravalent counterions, toroidal structures form and are stable. Fig. 4 shows the eight conformations. These conformations are not the same as the initial spiral structure. Along the central axis of

FIGURE 3 Equilibrated conformations of individual chains of $N = 256$ with $z_c = 2$ counterions using parameter set 2 (Table 1) and bond angle set 3 (Table 2). The initial conformation for each chain was a spiral.

the spiral the polyelectrolyte has contracted, and the circular turns have more than one diameter. The connection of this structure with energetics is discussed below.

The above results demonstrate that condensation of a polyelectrolyte is due solely to electrostatic interactions. No additional interactions are involved in the simulations. It is also clear that condensation can occur for a wide range of parameters: ξ, N, d, and L_p. The very long persistence lengths of DNA are not a requisite. However, multivalent ions with charge 3 or 4 are typically required (A simulation with $z_c = 3$ does find condensation). The condensed structures that form at $z_c = 4$ will now be discussed in more detail.

Condensed structure

It is not surprising that both toroidal and rod structures form. For homopolymers with varying stiffness in a poor solvent, it is known that both rod and toroidal structures form (Noguchi and Yoshikawa, 1998). When L_p is small (small k_1), the cost of a hairpin turn is relatively small, and rod structures are favored over toroids. As L_p increases, there is a transition to toroids. In semiflexible polyelectrolytes, the competition between rods and toroids depends on whether a few sharper turns require less energy than many slight bends, or whether the rod structure has a lower Coulomb energy, offsetting the additional cost of the angular term.

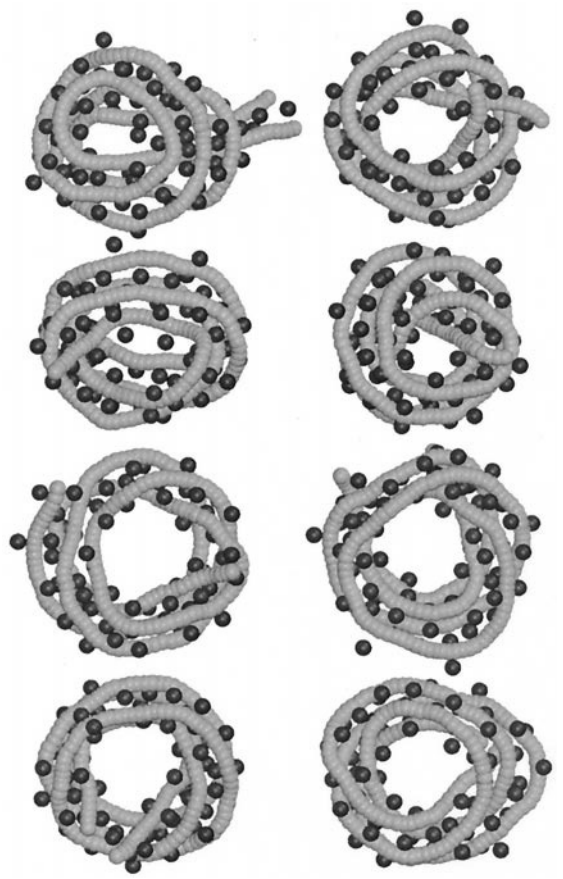

FIGURE 4 Images of toroidal structures for $N = 256$ molecules (*light spheres*) with $z_c = 4$ counterions (*dark spheres*) using parameter set 2 (Table 1) and bond angle set 3 (Table 2). The initial conformation for each chain was a spiral.

To examine the competition between rods and toroids, simulations similar to that of Fig. 5 were performed, but with parameter set 2 (Table 1), longer chains $N = 256$, and larger L_p ($k_1 = 20\ \epsilon/\text{rad}^2$). Fig. 5 shows all eight molecules condensed into twisted rod structures. Close examination of the hairpin turns in Fig. 5 shows that the turns are not true hairpins; rather, each bend is several monomers long. The innermost turns are the sharpest and the differential bond angle, $\Delta\theta = \theta - \theta_0$, is typically $<40°$. Other bends in the structure wrap around the inner segments and consequently are much less sharp. Thus, the angular energy in the rod's turns is not as expensive as might initially be expected.

There also appears to be a kinetic preference for hairpin turns in these cases, with k_1 not prohibitively large. The structures in Fig. 5 start with the formation of single hairpin turn, typically near the polymer end. The kinetic preference for the hairpin is due to relatively few monomers needed in the initial formation. When two segments of the polymer are parallel with counterions in between them, the Coulomb energy is significantly reduced. Once the hairpin turn has occurred, the energy is further decreased as the position of

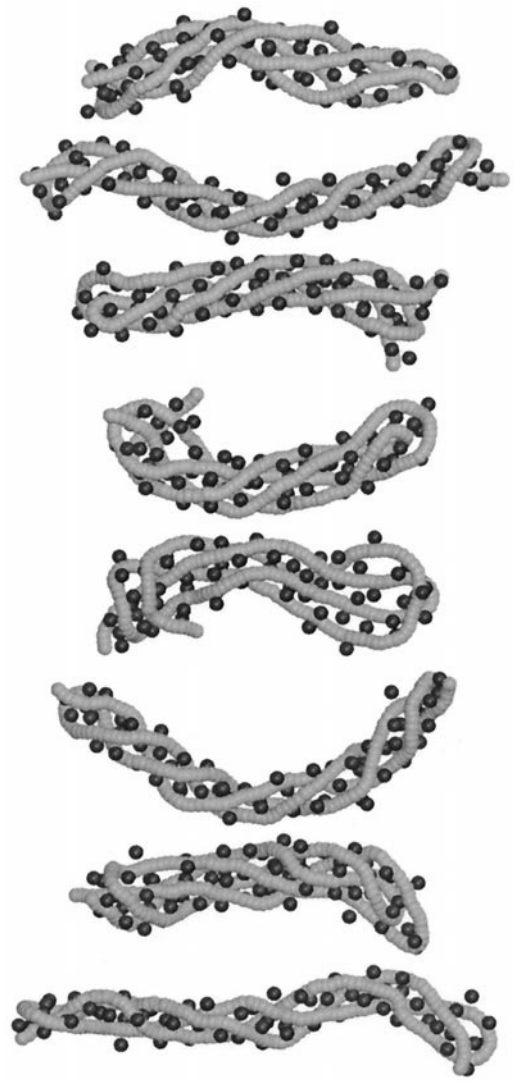

FIGURE 5 Images of rod structures for $N = 256$ molecule (*light spheres*) with $z_c = 4$ counterions (*dark spheres*). This is system 2 in Table 3.

the hairpin turn progressively moves, so that the parallel segments comprise more and more of the polyelectrolyte. In contrast, for toroid formation a complete circle must occur within the polymer before the Coulomb energy is lowered. This requires a larger number of monomers to be involved in the initial transition. The transition time is then longer for toroids, or, equivalently, the formation rate is lower for toroids. In the system of Fig. 5, the first hairpin turn occurs at about $t = 4500\ \tau$. The first complete rod structure occurs by 6000 τ. It takes 33,000 τ for all the chains to achieve their final rod structure.

Although rod structures have been observed for DNA (Bloomfield, 1996; Fang and Hoh, 1999), toroids are the typical condensate structure. Although the model system has a large bond bending stiffness relative to the bond length, L_p is small compared to that in DNA. For DNA the total persistence length is 240 basepairs (Calladine and Drew, 1997) or 480 charged monomers. For such a large persistence length, the maximum bend per monomer is at most a few degrees, precluding hairpins. In addition, for DNA it is not likely that the bending potential is harmonic at large bends. In the bead-spring model, the bond bending corresponds not to the bending of individual bonds within a DNA molecule, but to bending of the whole molecule.

The large angle bends can be made prohibitively expensive by including a quartic term in the bond bending potential, as is given in Eq. 8. The bond angle parameters in set 3 (Table 2) yield a potential similar to that of set 2 at small angles while making large angle bends more expensive. As already shown in Fig. 4, the toroid structure is stable for this parameter set. Although the hairpins appear kinetically favored in these simulations, the lowest energy state has not been determined. Between the toroidal and hairpin structures, the energies can be compared to determine the state with the lower energy.

To compare the energies of the toroid and rod states, simulations with identical parameters (i.e., bond angle potentials) must be performed, but for the two different conformations. Using the conformations in Figs. 4 and 5 as the starting configurations enables the calculations of their respective energy. In addition, the effect of increased molecular stiffness on the rod structures has been investigated. As the stiffness is increased, the toroidal structure will become more favorable. If the polymer length is long enough, the toroidal structure will in fact become the thermodynamic state (Noguchi and Yoshikawa, 1998).

To change the polymer stiffness, the quartic term in the bond angle potential (Eq. 8) is varied. As discussed above, increasing this term reduces the likelihood of large angle bends. Starting from parameter set 2 (Table 1) and bond angle set 2 (Table 2) for which the hairpins formed, the value of k_2 is increased. Fig. 6 shows how specific k_2 values are chosen. The solid line is for the bond angle potential set 2. The dotted lines are for the harmonic version ($k_2 = 0$) with $k_1 = 100$ and 200 ϵ/rad^2. For the dotted curves there would be no condensates at $N = 256$, since L_p is too large; these potentials are thus not used. By adding a quartic term to the bond angle set 2, the large angle bends can be progressively removed, as they would be for the large k_1 potentials, whereas the small angle bends will have the same energy. The value of k_2 is chosen so that U_{angle} is equal to the harmonic potential at $\Delta\theta = 20°$. To fit the $k_1 = 100$ ϵ/rad^2 line at $\Delta\theta = 20°$, the value of k_2 must be 650 ϵ/rad^4 with $k_1 = 20$ ϵ/rad^2. Similarly, to fit the $k_2 = 200$ ϵ/rad^2

TABLE 2 Bond angle parameters

Set	k_1 (ϵ/rad^2)	k_2 (ϵ/rad^4)
1	10	0
2	20	0
3	5	200

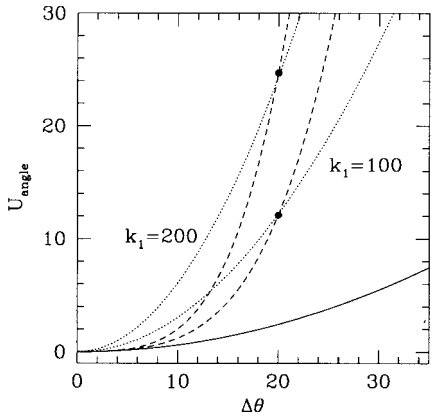

FIGURE 6 The bond angle potential for various parameters is shown. The *solid line* and the two *dotted lines* are harmonic ($k_2 = 0$). The *solid line* represents bond angle set 2 ($k_1 = 20\ \epsilon/\text{rad}^2$), and the *dotted* lines are labeled. The *dashed lines* have the same k_1 as the *solid line*, and k_2 is chosen to fit the *dotted lines* at $\Delta\theta = 20°$ (marked by *dots*).

line, $k_2 = 1500\ \epsilon/\text{rad}^4$. These potentials should alter the hairpin structure of Fig. 5. The simulations will determine whether these bond angle parameters are strong enough to cause the transition to toroids.

Table 3 gives the energies per particle for the different starting states and different bond angle parameters. System 1 is for the toroidal structure. The potential energy for the toroid structure is the lowest of all the structures. Compared to the rod system of Fig. 5 (System 2), the toroidal structure of Fig. 4 has a higher Coulomb energy but a lower bond angle energy; the net effect is that the toroid potential energy is lower. Table 3 gives the energies for the rod structures as k_2 increases. As k_2 increases, the bond angle potential energy decreases, which was not expected. However, this energy decrease occurs because the conformations change. The diameter of the turns in the structure increases such that the turns are no longer hairpins, but have a diameter smaller than the toroid loops. The structures in systems 3 and 4 do not evolve into toroids. Instead, they remain elongated, but now with large loops at the ends wider than the more compact middle sections of parallel segments. The twisted nature of the rod disappears in system 4.

For system 5 (Fig. 7), the final structure depends on the initial rod structure. Some molecules become toroids; some remain rods; some look like tennis racquets with a large loop at one end and a rod at the other end (cf. Schurr et al., 1999). In the starting rod structures (Fig. 5) there are two structural subsets. One set has the molecule ends at different rod ends and 3 middle parallel segments; the other has the molecule ends at the same rod end and 4 middle parallel segments. The rods with 3 segments remains rods as k_2 is increased, but the rods with 4 segments become toroids or tennis racquets. With 4 segments, the transition to a toroid can occur continuously by having the center open up, with 2 segments going to the left and 2 going to the right. The rods with 3 segments cannot continuously transform into a

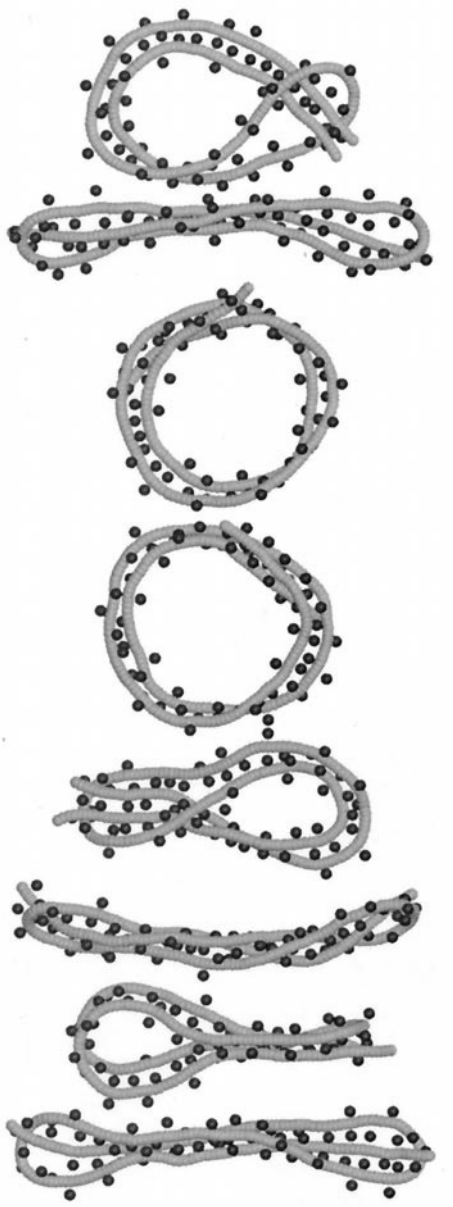

FIGURE 7 Images of structures for $N = 256$ molecules (*light spheres*) with $z_c = 4$ counterions (*dark spheres*). This is for system 5 in Table 3, which had Fig. 5 as its starting state.

TABLE 3 Energy comparison

System	Total PE	Coulomb	Angle	Bond	LJ	k_1	k_2
1	−2.84	−8.27	0.80	4.38	0.26	20	650
2	−2.73	−8.47	1.09	4.37	0.26	20	0
3	−2.73	−8.21	0.86	4.37	0.25	20	300
4	−2.65	−8.11	0.84	4.37	0.25	20	650
5	−2.62	−7.97	0.78	4.35	0.25	20	1500

Energy in units of ϵ.

toroidal structure. Two segments going to the left would leave only 1 segment going to the right and an unbalanced situation. The 3-segment rod would first have to become an extended chain and then recondense into a toroid. In this case, the kinetic barrier is too high. The configurations are shown at about $t = 80{,}000\ \tau$. In a similar manner, the tennis racquet structures occur for the 4-segment molecule, in which the free ends have paired up and have not gone to separate sides of the loop. This makes the rod structure more stable; there is effectively an entanglement at the racquet handle. Presumably if the simulation were run long enough, these molecules would transform into a complete toroid.

Overall, the clear trend in increasing k_2 for the systems with the rod starting states is that the Coulomb energy decreases monotonically. The bond angle energy also decreases, but the majority of this decrease occurs once $k_2 > 0$. The decrease in the Coulomb energy is related to the larger separation of the charges particularly at the turns in the rod. The toroid structure has the lowest energy of all states, and by increasing k_2 a transition to toroids does occur. There are clear kinetic barriers associated with specific initial structures so that rod structures can be strong metastable states.

Charge ordering of polyelectrolyte condensation

The ordering of charged monomers and counterions involved in toroidal structures compared to extended, noncondensed polyelectrolyte structure can be seen in radial distribution functions (rdf). Fig. 8 shows both the monomer-counterion rdf, $g_{mc}(r)$, and the counterion-counterion rdf, $g_{cc}(r)$, for both structures. Because of the strong counterion condensation due to tetravalent counterions, the peaks are very large in the figure. Because the molecular condensation process is rather slow on the simulation time scale, simulations that start with extended structures easily remain extended long enough for calculation of $g(r)$ in this state. The rdf curves for the noncondensed state are rather structureless, and the only feature is due to counterion condensation. The single, large peak at contact in $g_{mc}(r)$ is due to the condensed counterions, which spend most of the time right next to the polymer. Because there are so many counterions on the polymer, the counterion-counterion rdf exhibits a peak at about 5.7 σ, corresponding to the average separation along the polymer between neighboring counterions. For $z_c = 4$, all the counterions condense, yielding a counterion for every z_c monomers. The separation of charged monomers is 1.1 σ, giving a distance of 4.4 σ between neighboring condensed counterions, if they were on the same side of the polyelectrolyte. This is not a very favorable position due to the Coulomb repulsion between counterions, and $g_{cc}(4.4\ \sigma) \simeq 0$ confirms this point. If the counterions were on opposite sides of the polyelectrolyte, then the separation distance would be 6.2 σ, which is slightly larger than the peak position. The smaller value of the peak position corresponds to the distribution of positions, with the most probable being close to that of counterion on opposite sides.

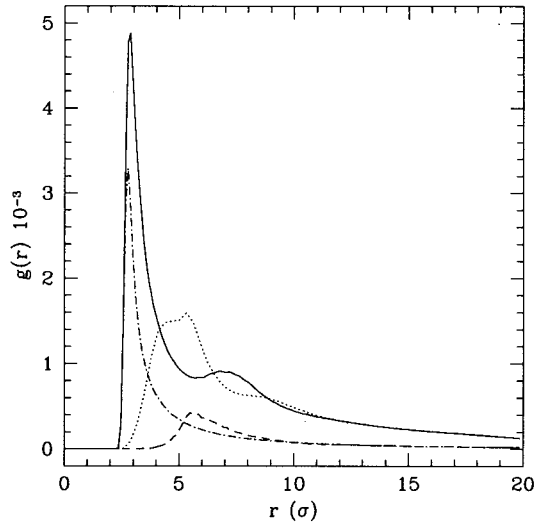

FIGURE 8 The monomer-counterion and the counterion-counterion radial distribution functions (rdf) for the toroid structure (Fig. 4) and for the extended, noncondensed structure. Both systems have tetravalent counterions. The *solid line* is the monomer-counterion rdf for the toroids; the *dot-dashed line* is for the noncondensed structure. The *dotted line* is the counterion-counterion rdf for the toroids; the *dashed line* is for the noncondensed structure.

For toroids (and rods), both distribution functions exhibit structure beyond just counterion condensation. Moreover, this structure is a result of charge ordering due to condensate structure. For example, in $g_{mc}(r)$ for the toroids, a second peak appears at about 7.2 σ. This peak is due to counterions condensed on a neighboring loop in the toroid. To simplify the notation, let *c* stand for counterion and *m* for monomer. Then, the peak at 7.2 σ corresponds to the sequence *m-c-m-c*, where the first *m* is the central monomer, the first *c* is its condensed counterion, the second *m* is a monomer of a neighboring loop, and the last *c* is a condensed counterion to this neighboring loop. The straight line separation between the central monomer and the last counterion is $3d = 7.9\ \sigma$. The peak position is smaller than $3d$, implying that the *m-c-m-c* sequence tends not to be straight, but zig-zagged, as in a triangular lattice. This more compact structure lowers the Coulomb energy.

The $g_{cc}(r)$ for the toroids is the most interesting of all the distributions. Besides the peak at 5.7 σ, which occurs in the noncondensed state, there are two additional peaks. There is now a peak at 4.4 σ as well as a discernable but relatively weak peak at about 9.5 σ. The peak at 4.4 σ was noted above to be just the separation distance between counterions on the same side of the polymer. In the noncondensed state, this ordering is unfavorable. In the toroid structure, this ordering becomes favorable, because the counterion is shared among multiple loops of the toroid. The peak at large

$r = 9.5\ \sigma$ is the correlation between counterions with two loops in between. In the notation above, the sequence is *c-m-c-m-c*. A straight arrangement would give the peak at $4d = 10.5\ \sigma$. Again, the peak position implies that the arrangement is more compact.

From Fig. 8, the charge-ordered sequence *c-m-c-m-c* is clearly resolvable. Such charge ordering is the favored structure by the Coulomb interactions, because the Coulomb energy is lowered. Such structure can form when the Coulomb interactions dominate entropic interactions. DNA condensates form because these charge-ordered states are more stable and have lower energy than extended structures when the Coulomb interactions are sufficiently strong (i.e., $z_c \geq 3$).

The charge-ordered state corresponds to the collapsed state at large Γ in the OCP picture. Condensation occurs when the Coulomb interactions are strong enough to stabilize charge-ordered structures such as toroids or rods. For $z_c \geq 3$ and typical diameters, the Coulomb interactions are strong enough for condensation. However, for $z_c \leq 2$, entropy is dominant, and condensates are not stable.

CONCLUSIONS

Molecular dynamics simulations of a simple, bead-spring model of semiflexible polyelectrolytes such as DNA have been performed to study condensation. Starting from extended polymer conformations, condensation into toroids and rods occurs in the molecular dynamics simulations. Condensates form for tetravalent and trivalent counterions, but not divalent counterions. Besides treating the charge density of DNA, various polymer lengths, polymer stiffnesses, charge densities, and monomer sizes were simulated and produced condensates. Condensation is a generic phenomenon of semiflexible polyelectrolytes. Furthermore, condensation is primarily an electrostatic phenomenon. For condensation to occur, the Coulomb interactions must be stronger than the entropic interactions to overcome the entropic loss of condensation. For this reason, multivalent ions of valence of at least 3 are typically required. When the Coulomb interactions are strong enough to dominate the entropic interactions, the polyelectrolyte, along with its counterions, forms a charge-ordered structure. This structure is either a toroid or a rod, depending on the stiffness of the polymer (assuming $L_p \ll L$). Toroidal structures are favored by the large persistence lengths found in molecules like DNA.

It is very important biologically that the condensation mechanism is independent of the basepair sequence and, more generally, the chemistry of DNA. Fitting DNA into small packages must be done independent of the genetic code it contains. Otherwise, some genetic sequences could not exist. The mechanism described here depends solely on electrostatic interactions of the DNA phosphates and the counterions.

This work was supported by the U. S. Department of Energy under contract DE-AC04–94AL8500. Sandia is a multiprogram laboratory operated by Sandia Corp., a Lockheed Martin Company, for the Department of Energy.

REFERENCES

Baus, M., and J. P. Hansen. 1980. Statistical mechanics of simple Coulomb systems. *Phys. Rep.* 59:2–94.

Brami, B., J. P. Hansen, and F. Joly. 1979. Phase separation of highly disymmetric binary ionic mixtures. *Physica.* 95A:505–525.

Bloomfield, V. A. 1991. Condensation of DNA by multivalent cations: consideration on mechanism. *Biopolymers.* 31:1471–1481.

Bloomfield, V. A. 1996. DNA condensation. *Curr. Opin. Struct. Biol.* 6:334–341.

Brilliantov, N. V., D. V. Kuznetsov, and R. Klein. 1998. Chain collapse and counterion condensation in dilute polyelectrolyte solutions. *Phys. Rev. Lett.* 1433:81–84.

Calladine, C. R., and H. R. Drew. 1997. Understanding DNA. Academic Press, San Diego, CA.

Grønbech-Jensen, N., R. J. Mashl, R. F. Bruinsma, and W. M. Gelbart. 1997. Counterion-induced attraction between rigid polyelectrolytes. *Phys. Rev. Lett.* 78:2477–2480.

Ha, B.-Y., and A. J. Liu. 1997. Counterion-mediated attraction between two like-charged rods. *Phys. Rev. Lett.* 79:1289–1292.

Hockney, R. W., and J. W. Eastwood. 1988. Computer Simulation Using Particles. Adam Hilger, New York.

Fang, Y., and J. Hoh. 1998. Early intermediates in spermidine-induces DNA condensation on the surface of mica. *J. Am. Chem. Soc.* 120: 8903–8909.

Fang, Y., and J. H. Hoh. 1999. Cationic silanes stabilize intermediates in DNA condensation. *FEBS Lett.* 459:173–176.

Kjellander, R., and S. Marčelja. 1984. *Chem. Phys. Lett.* 112:49–53.

Kleinschmidt, A. K. D. Land, D. Jacherts, and R. K. Zahn. 1962. Darstellung und Längenmessungen des gesamten desoxyribonucleinsäureinhaltes von t_2-Bakteriophagen. *Biochim. Biophys. Acta.* 61:857–864.

Lyubartsev, A. P., and L. Nordenskiöld. 1995. Monte Carlo simulation study of polyelectrolyte properties in the presence of multivalent polyamine ions. *J. Polymer Chem. B.* 101:4335–4342.

Kremer, K., and G. S. Grest. 1990. Dynamics of entangled linear polymer melts: a molecular-dynamics simulation. *J. Chem. Phys.* 92:5057–5086.

Manning, G. 1969. Limiting laws and counterion condensation in polyelectrolyte solutions I. Colligative properties. *J. Chem. Phys.* 51: 924–933.

Neu, J. C. 1999. Wall-mediated forces between like-charged bodies in an electrolyte. *Phys. Rev. Lett.* 82:1072–1074.

Noguchi, H., and K. Yoshikawa. 1998. Morphological variation in a collapsed single homopolymer chain. *J. Chem. Phys.* 109:5070–5077.

Oosawa, F. 1971. Polyelectrolytes. Marcel Dekker, New York.

Pollock, E. L., and J. Glosli. 1996. Comments on p3.m, fmm and the Ewald method for large periodic coulombic systems. *Comput. Phys. Commun.* 95:93–110.

Ray, J., and G. S. Manning. 1994. Fluctuations of counterions condensed on charged polymers. *Langmuir.* 10:962–966.

Sader, J. E., and D. Y. C. Chan. 1999. Long-range electrostatic attractions between identically charged particles in confined geometries: an unresolved problem. *J. Colloid Interface Sci.* 213:268–269.

Schiessel, H., and P. Pincus. 1998. Counterion-condensation-induced collapse of highly charged polyelectrolytes. *Macromolecules.* 31: 7953–7959.

Schneider, T., and E. Stoll. 1978. Molecular-dynamics study of a 3-dimensional one-component model for distortive phase-transitions. *Phys. Rev. B.* 17:1302–1322.

Schurr, B., F. Gittes, F. C. MacKintosh, and D. R. M. Williams. 1999. Collapse dynamics of biopolymers with attractive interactions: the transition to toroids via tennis racquets. *Biophys. J.* 76:A245–A245.

Stevens, M. J. 1999. Bundle binding in polyelectrolyte solutions. *Phys. Rev. Lett.* 82:101–104.

Stevens, M. J., and K. Kremer. 1995. Structure of salt-free linear polyelectrolytes. *J. Chem. Phys.* 103:1669–1690.

Stevens, M. J., and M. O. Robbins. 1990. Density functional theory of ionic screening: when do like charges attract. *Europhys. Lett.* 12:81–86.

Stevens, M. J., M. L. Falk, and M. O. Robbins. 1996. Interactions between charged spherical macroions. *J. Chem. Phys.* 104:5209–5219.